Journal of Ceramic Processing Research. Vol. 15, No. 4, pp. 246~250 (2014)

J O U R N A L O F
Ceramic Processing Research

Simultaneously rapid synthesis and consolidation of nanostructured $MgAl_2Ti_3O_{10}$-$Mg_{0.6}Al_{0.8}Ti_{1.6}O_5$ composite and its mechanical properties

Hyun-Su Kang[a], Jung-Mann Doh[b], Jin-Kook Yoon[b], Seok-Jae Lee[a] and In-Jin Shon[a,*]

[a]*Division of Advanced Materials Engineering and the Research Center of Advanced Materials Development, Engineering College, Chonbuk National University, 561-756, Korea*

[b]*Interface Control Research Center, Korea Institute of Science and Technology, PO Box 131, Cheongryang, Seoul 130-650, Korea*

Nanocrystalline materials have received much attention as advanced engineering materials with improved physical and mechanical properties. As nanomaterials possess high strength, high hardness, excellent ductility and toughness, undoubtedly, more attention has been paid to the application of nanomaterials. Nanopowders of Al_2O_3, TiO_2 and MgO were fabricated by high energy ball milling. The simultaneous synthesis and sintering of nanostuctured $MgAl_2Ti_3O_{10}$-$Mg_{0.6}Al_{0.8}Ti_{1.6}O_5$ composite from milled powders of $1.4Al_2O_3$, $4.6TiO_2$ and 1.6MgO was investigated by the high-frequency induction heated sintering process. A highly dense nanostructured $MgAl_2Ti_3O_{10}$-$Mg_{0.6}Al_{0.8}Ti_{1.6}O_5$ composite was produced with the simultaneous application of 80 MPa pressure and an induced current within one minute. The grain sizes and mechanical properties (hardness and fracture toughness) of $MgAl_2Ti_3O_{10}$-$Mg_{0.6}Al_{0.8}Ti_{1.6}O_5$ composite sintered at 1100 °C were investigated.

Key words: Synthesis, Sintering, Composite, Nanostructured material, Powder metallurgy.

Introduction

The oxide synthesized from MgO-Al_2O_3-TiO_2 system is one of the excellent dielectric materials widely used in ceramic package [1, 2], for its low dielectric constant and low dielectric loss [3]. In recent 20 years it has been extensively investigated [4, 5]. With the development of wireless telecommunication, dielectric materials with controllable dielectric constant are required in the design of microwave circuit to realize different function. However, as in the case of many ceramic materials, the current concern about these materials focuses on their low fracture toughness below the ductile-brittle transition temperature [6, 7]. To improve their mechanical properties, the approach commonly utilized has been the addition of a second phase to form composites and to make nanostructured materials.

Nanocrystalline materials have received much attention as advanced engineering materials with improved physical and mechanical properties [8, 9]. As nanomaterials possess high strength, high hardness, excellent ductility and toughness, undoubtedly, more attention has been paid to the application of nanomaterials [10, 11]. In recent days, nanocrystalline powders have been developed by the thermochemical and thermomechanical process named as the spray conversion process (SCP), co-precipitation and high energy milling [12~14]. The sintering temperature of high energy mechanically milled powder is lower than that of unmilled powder due to the increased reactivity, internal and surface energies, and surface area of the milled powder, which contribute to its so-called mechanical activation [15-17]. However, the grain size in sintered materials becomes much larger than that in pre-sintered powders due to a rapid grain growth during a conventional sintering process. Therefore, even though the initial particle size is less than 100 nm, the grain size increases rapidly up to 2 μm or larger during conventional sintering [18]. So, controlling grain growth during sintering is one of the keys to the commercial success of nanostructured materials. In this regard, the high-frequency induction heated sintering method (HFIHSM) which can make dense materials within 2 minutes has been shown to be effective in achieving this goal [19-21].

In this study, we investigated the simultaneous synthesis and consolidation of $Mg_2Al_6Ti_7O_{25}$-$Mg_{0.6}Al_{0.8}$ $Ti_{1.6}O_5$ composite from milled $1.4Al_2$ O_3 + 1.6MgO + $4.6TiO_2$ powders by the HFIH method. The goal of this research is to produce dense nanostructured $MgAl_2$ Ti_3O_{10}-$Mg_{0.6}$ $Al_{0.8}$ $Ti_{1.6}O_5$ composite. In addition, we also studied the microstructure and mechanical properties of $MgAl_2Ti_3$ O_{10}-$Mg_{0.6}Al_{0.8}Ti_{1.6}O_5$ composite.

Experimental Procedure

The MgO powder with a grain size of < 45 μm and 99.8% purity and Al_2O_3 powder with a grain size of < 3 μm and 99.99% purity and TiO_2 powder with a grain size of < 45 μm and 99.8% purity used in this research was supplied by Alfa. The powders (1.4MgO-

*Corresponding author:
Tel : +82-63-270-2381
Fax: +82-63-270-2386
E-mail: ijshon@chonbuk.ac.kr

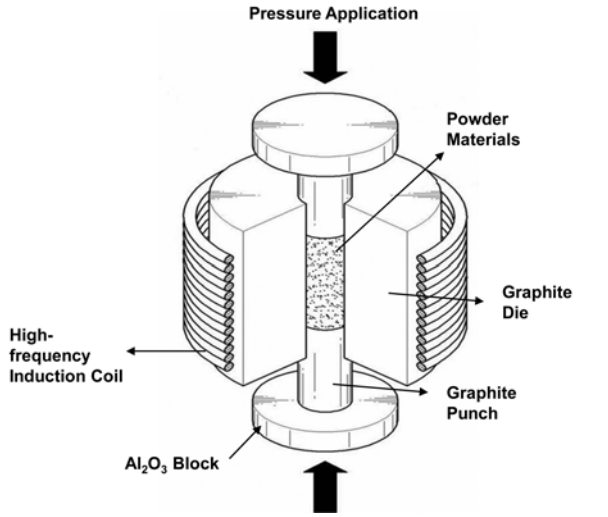

Fig. 1. Schematic diagram of apparatus for high-frequency induction heated sintering.

$1.6Al_2O_3$-$4.6TiO_2$) were first milled in a high-energy ball mill (Pulverisette-5 planetary mill) at 250 rpm for 10 h. Tungsten carbide balls (9 mm in diameter) were used in a sealed cylindrical stainless steel vial under an argon atmosphere.

The powders were placed in a graphite die (outside diameter, 35 mm; inside diameter, 10 mm; height, 40 mm) and then introduced into the high-frequency induction heated sintering (HFIHS) apparatus shown schematically in fig. 1. The HFIHS apparatus includes a 15 kW power supply which provides a induced current with 50 kHz frequency through the sample, and a 50 kN uniaxial load. The system was first evacuated and a uniaxial pressure of 80 MPa was applied. A induced current was then activated and maintained until the densification rate was negligible, as indicated by the real-time output of the shrinkage of the sample. The shrinkage was measured by a linear gauge measuring the vertical displacement. Temperatures were measured by a pyrometer focused on the surface of the graphite die. At the end of the process, the induced current was turned off and the sample cooled to room temperature. The process was carried out under a vacuum of 5.33 Pa.

Microstructural information was obtained from product samples, which had been polished and etched using thermal etching for 1 h at 1000 ºC. Compositional and microstructural analyses of the products were made through X-ray diffraction (XRD), and a field emission scanning electron microscope (FE-SEM) with energy dispersive X-ray spectrometer (EDS). Vickers hardness was measured by performing indentations at a load of 5 kg and a dwell time of 15 s. The grain sizes of the powders and sintered products were calculated from the full width at half-maximum (FWHM) of the diffraction peak by Suryanarayana and Grant Norton's formula [22]:

$$B_r(B_{crystalline} + B_{strain})\cos\theta = k\,\lambda / L + \eta\sin\theta \quad (1)$$

where B_r is the full width at half-maximum (FWHM) of the diffraction peak after instrumental correction; $B_{crystalline}$ and B_{strain} are the FWHM caused by a small grain size and internal stress, respectively; k is a constant (with a value of 0.9); λ is the wavelength of the X-ray radiation; L and η are the grain size and internal strain, respectively; and θ is the Bragg angle. The parameters B and B_r follow Cauchy's form with the relationship: $B = B_r + B_s$, where B and B_s are the FWHM of the broadened Bragg peaks and the standard sample's Bragg peaks, respectively.

Results and Discussion

Fig. 2 shows X-ray diffraction patterns of the MgO, TiO_2 and Al_2O_3 powders after high-energy ball milling for 10h. Only MgO, TiO_2 and Al_2O_3 peaks are detected and product peaks of $MgAl_2Ti_3O_{10}$ and $Mg_{0.6}Al_{0.8}Ti_{1.6}O_5$ are not detected. Therefore, it is obvious that no chemical reaction occurred between the component powders during milling. Nevertheless, the peaks of the powders are significantly wide suggesting that their crystallize sizes became very fine by milling. Fig. 3 shows a plot of $B_r\cos\grave{e}$ versus $\sin\grave{e}$ of TiO_2 , MgO and Al_2O_3 milled for 10 h to calculate the particle size from XRD data. The average grain sizes of the milled TiO_2, MgO and Al_2O_3 powders determined by Suryanarayana and Grant Norton's formula were about 14, 19 and 18 nm, respectively.

FE-SEM images of MgO, TiO_2 and Al_2O_3 powders after milling for 10 h are shown in fig. 4. MgO, TiO_2 and Al_2O_3 powders have a round shape, refinement with milling and some agglomeration. In EDS, Al, Si, Mg, Pt and O peaks are detected. It is considered that Pt comes from coating to observe mocrostructure of powders. The milling process is known to introduce impurities from the ball and/or container. However, in this study, peaks of W and Fe were not identified.

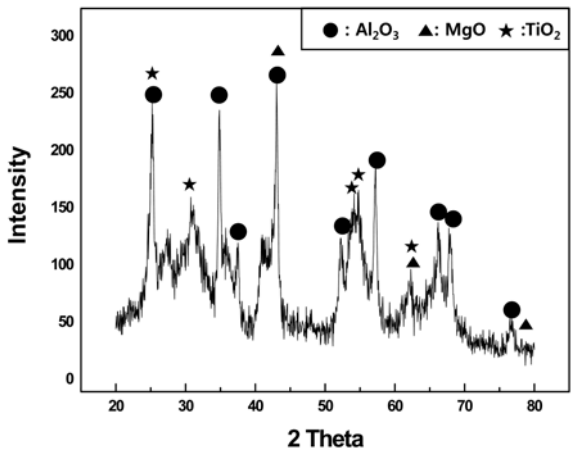

Fig. 2. X-ray diffraction patterns of the TiO_2, Al_2O_3 and MgO powders milled for 10 h.

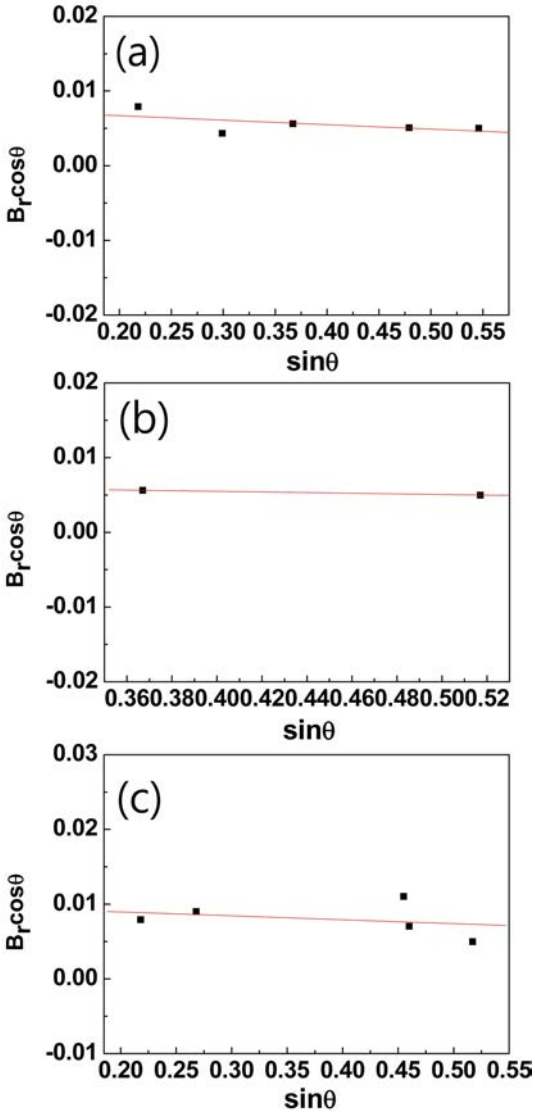

Fig. 3. Plot of B_r ($B_{crystalline} + B_{strain}$) cosθ versus sinθ for Al_2O_3 (a), MgO (b) and TiO_2 (c) powder milled for 10 h.

The variations of the shrinkage displacement and temperature with the heating time for induced current during the sintering of the high energy ball milled MgO, TiO_2 and Al_2O_3 powders under a pressure of 80 MPa are shown in fig. 5. The application of the induced current resulted in shrinkage due to consolidation. As the induced current was applied, shrinkage displacement was nearly constant up to 550 ºC. And then the shrinkage abruptly increased at the above temperature. Fig. 6 shows the XRD pattern of a specimen sintered at 1100 ºC from the high energy ball milled MgO, TiO_2 and Al_2O_3 powders. In fig. 6, $MgAl_2Ti_3O_{10}$ and $Mg_{0.6}Al_{0.8}Ti_{1.6}O_5$ peaks are detected. From the X-ray diffraction, the interaction between these phases, i.e.,

$$1.4Al_2O_3 + 1.6MgO + 4.6TiO_2 \rightarrow MgAl_2Ti_3O_{10} + Mg_{0.6}Al_{0.8}Ti_{1.6}O_5 \quad (2)$$

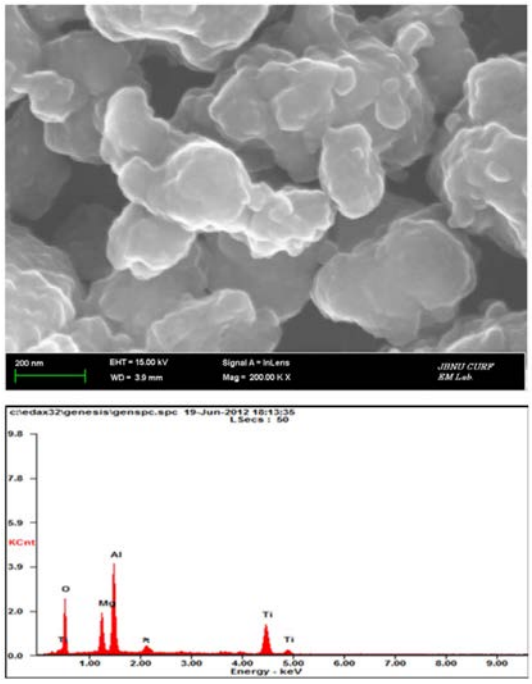

Fig. 4. FE-SEM image and EDS of the TiO_2, Al_2O_3 and MgO powders milled for 10 h.

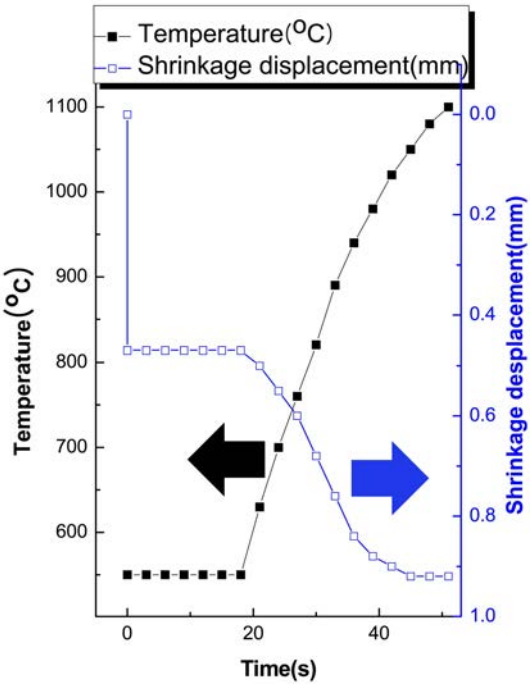

Fig. 5. Variations of temperature and shrinkage with heating time during the synthesis and sintering of $4.6TiO_2 + 1.4Al_2O_3 + 1.6$ MgO powders milled for 10 h.

is thermodynamically feasible.

The abrupt increase in the displacement of shrinkage at the ignition temperature in fig. 5 is due to the increase in density as a result of the molar volume change associated with the formation of $MgAl_2Ti_3O_{10} + Mg_{0.6}Al_{0.8}Ti_{1.6}O_5$ from $1.4Al_2O_3 + 1.6MgO + 4.6TiO_2$ reactant and the

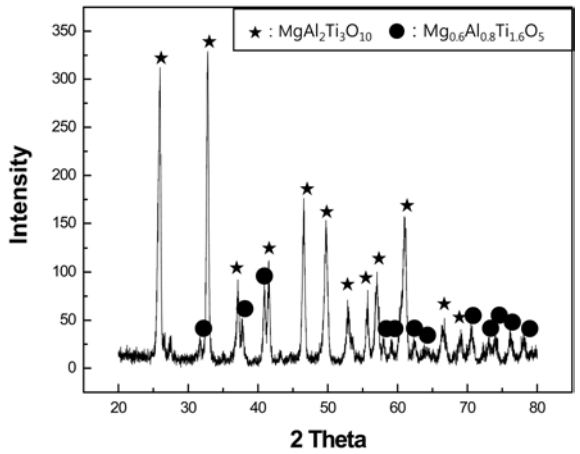

Fig. 6. XRD pattern of specimen of sintered $MgAl_2Ti_3O_{10}$-$Mg_{0.6}Al_{0.8}Ti_{1.6}O_5$ composite from the high energy ball milled $4.6TiO_2 + 1.4Al_2O_3 + 1.6$ MgO powders.

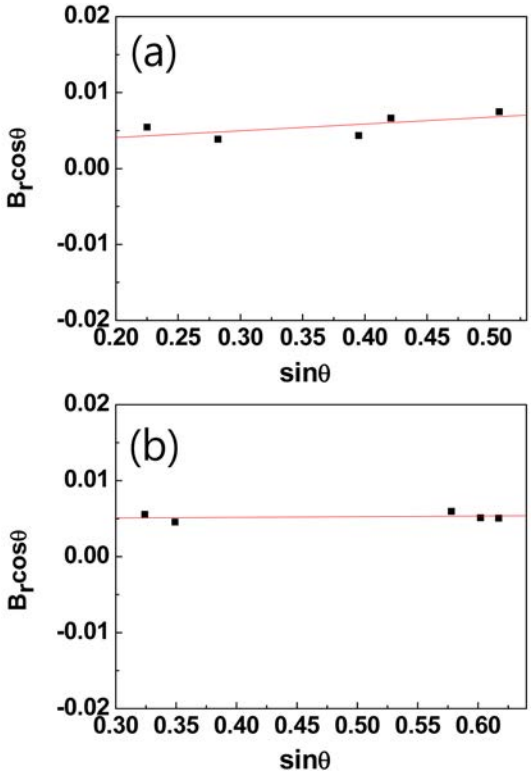

Fig. 7. Plot of B_r ($B_{crystalline} + B_{strain}$) cosθ versus sinθ for $MgAl_2Ti_3O_{10}$ (a) and $Mg_{0.6}Al_{0.8}Ti_{1.6}O_5$ (b) in composite sintered from the $4.6TiO_2 + 1.4Al_2O_3 + 1.6$ MgO powders milled for 10 h.

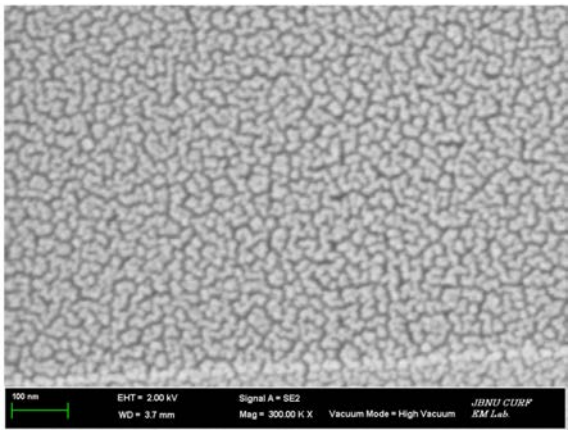

Fig. 8. FE-SEM image of sintered $MgAl_2Ti_3O_{10}$– $Mg_{0.6}Al_{0.8}Ti_{1.6}O_5$ composite.

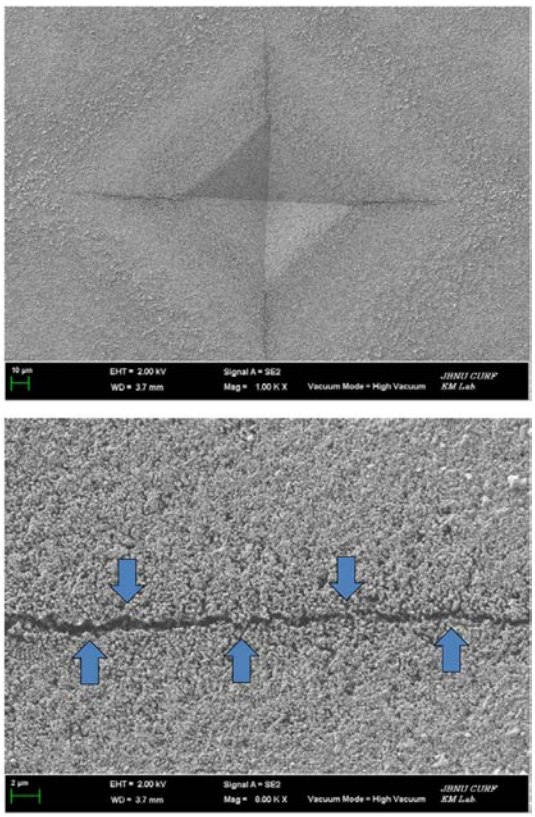

Fig. 9. Vickers indentation (a) and crack propagating (b) in the $MgAl_2Ti_3O_{10}$-$Mg_{0.6}Al_{0.8}Ti_{1.6}O_5$ composite sintered from milled $4.6TiO_2 + 1.4Al_2O_3 + 1.6$ MgO powders.

consolidation of the product.

Fig. 7 shows plot of $B_r\cos\theta$ versus sinθ for $MgAl_2Ti_3O_{10}$ and $Mg_{0.6}Al_{0.8}Ti_{1.6}O_5$ in Suryanarayana and Grant Norton's formula [22]. The average grain size of the $MgAl_2Ti_3O_{10}$ and $Mg_{0.6}Al_{0.8}Ti_{1.6}O_5$ calculated from the XRD data using Suryanarayana and Grant Norton's formula was about 60 and 28 nm. Thus, the average grain size of the sintered $MgAl_2Ti_3O_{10}$ and $Mg_{0.6}Al_{0.8}Ti_{1.6}O_5$ is not larger than that of the initial powders, indicating the absence of substantial grain growth during sintering. This retention of the grain size is attributed to the high heating rate and the relatively short term exposure of the powders to the high temperature. FE-SEM images of $MgAl_2Ti_3O_{10}$ and $Mg_{0.6}Al_{0.8}Ti_{1.6}O_5$ composite sintered from MgO, TiO_2 and Al_2O_3 powders milled for 10 h are shown in fig. 8. The $MgAl_2Ti_3O_{10}$ and $Mg_{0.6}Al_{0.8}Ti_{1.6}O_5$ consists of nanocrystallines.

The role of the current (resistive or inductive) in sintering and or synthesis has been the focus of several attempts aimed at providing an explanation of the

observed enhancement of sintering and the improved characteristics of the products. The role played by the current has been variously interpreted, the effect being explained in terms of a rapid heating rate due to Joule heating, the presence of a plasma in the pores separating powder particles, and the intrinsic contribution of the current to mass transport [23-26].

Vickers hardness measurements were performed on polished sections of the $MgAl_2Ti_3O_{10}$-$Mg_{0.6}Al_{0.8}Ti_{1.6}O_5$ composite using a 5 kg load and 15 s dwell time. The Vickers hardness of $MgAl_2Ti_3O_{10}$-$Mg_{0.6}Al_{0.8}Ti_{1.6}O_5$ composite sintered from Al_2O_3, TiO_2 and MgO powders milled for 10 h was 867 kg/mm^2. Indentations with large enough loads produced median cracks around the indent. Fig. 9(a) shows Vickers indentations in the $MgAl_2Ti_3O_{10}$-$Mg_{0.6}Al_{0.8}Ti_{1.6}O_5$ composite sintered from TiO_2-MgO-Al_2O_3 powders. One to three additional cracks were observed to propagate from the indentation corners. The length of these cracks permits an estimation of the fracture toughness of the materials by means of the expression [27]:

$$K_{IC} = 0.203(c/a)^{-3/2} \cdot H_v \cdot a^{1/2} \quad (3)$$

where c is the trace length of the crack measured from the center of the indentation, a is one half of the average length of the two indent diagonals, and H_v is the hardness. The calculated fracture toughness value for the $MgAl_2Ti_3O_{10}$-$Mg_{0.6}Al_{0.8}Ti_{1.6}O_5$ composite sintered from TiO_2-Al_2O_3-MgO powders is about 3.1 MP $\cdot$ am$^{1/2}$. As in the case of the hardness value, the toughness value is the average of five measurements. A higher magnification view of an indentation median crack in the $MgAl_2Ti_3O_{10}$-$Mg_{0.6}Al_{0.8}Ti_{1.6}O_5$ composite is shown in Figure 9(b), which shows that the crack propagated deflectively (↑). Unfortunately, the hardness and toughness values of $MgAl_2Ti_3O_{10}$-$Mg_{0.6}Al_{0.8}Ti_{1.6}O_5$ composite were not available in the literature. Therefore, the comparative evaluation of the mechanical properties of nanostructured $MgAl_2Ti_3O_{10}$-$Mg_{0.6}Al_{0.8}Ti_{1.6}O_5$ composite prepared in this study was not possible.

Summary

Nanopowders of TiO_2, Al_2O_3 and MgO were fabricated by high energy ball milling for 10h. Using the high-frequency induction heated sintering, the simultaneously rapid synthesis and densification of nanostuctured Mg $Al_2Ti_3O_{10}$-$Mg_{0.6}Al_{0.8}Ti_{1.6}O_5$ composite was accom-plished within one minute from mechanically activated powders (4.6TiO_2-1.4Al_2O_3-1.6 MgO) using high energy ball milling. The average grain size of the $MgAl_2Ti_3O_{10}$ and $Mg_{0.6}Al_{0.8}Ti_{1.6}O_5$ were about 60 and 28 nm. The Vickers hardness and fracture toughness of $MgAl_2$ Ti_3O_{10}-$Mg_{0.6}$ $Al_{0.8}Ti_{1.6}O_5$ composite sintered from TiO_2, Al_2O_3 and MgO powders milled for 10 h were 867 kg/mm^2 and 3.1 MP $\cdot$ am$^{1/2}$, respectively.

Acknowledgments

This work is partially supported by KIST Future Resource Research Program and this work was supported by the Human Resources Development program (No. 20134030200330) of the Korea Institute of Energy Technology Evaluation and Planning (KETEP) grant funded by the Korea government Ministry of Trade, Industry and Energy.

References

1. S.H. Knickerbocker, A.H. Kumar, L.W. Herron, Am. Ceram. Soc. Bull. 72 (1993) 90-95.
2. D.R. Bridged Holland, P.W. Mcmilan, Glass Technol. 26 (6) (1985) 286-292.
3. P.J. Howard, G. Partridge, Proc. Br. Ceram. 49 (1992) 37-41.
4. Shaohong Wang, Heping Zhou, Linghong Luo, Mater. Res. Bull. 38 (2003) 1367-1374.
5. A.H. Kumar, US Patent 4,301.324 (1981).
6. I.J. Shon, S.L. Du, J.M. Doh, J.K. Yoon, Met. Mater. Int., 19 (2013) 1041-1045.
7. S.M. Kwak, H.K. Park, I.J. Shon, Korean J. Met. Mater. 51 (2013) 341-348.
8. M. Sherif El-Eskandarany, J. Alloys & Compounds 305 (2000) 225-238.
9. L Fu, LH Cao, YS Fan, Scripta Materialia 44 (2001) 1061-1068.
10. K Niihara, A Nikahira, Advanced structural Inorganic Composite, Elsevier Scientific Publishing Co., Trieste, Italy, 1990.
11. S Berger, R Porat, R Rosen, Progress in Materials 42 (1997) 311-320.
12. Z Fang, JW Eason, Int. J. of Refractory Met. & Hard Mater 13 (1995) 297-303.
13. A.I.Y. Tok, L.H. Luo, F.Y.C. Boey, Materials Science and Engineering A 383 (2004) 229-234.
14. I.J. Shon, I.Y. Ko, H.S. Kang, K.T. Hong, J.M. Doh, J.K. Yoon, Met. Mater. Inter. 18 (2012) 109-113.
15. I.Y. Ko, N.R. Park, I.J. Shon, Korean J. Met. Mater. 50 (2012) 369-374.
16. G.W. Lee, I.J. Shon, Korean J. Met. Mater. 51 (2013) 95-100.
17. Na-Ra Park, Kwon-Il Na, Hanjung Kwon, Jae-Won Lim, and In-Jin Shon, Korean J. Met.Mater. 51, (2013) 753-759.
18. J. Jung, S. Kang, Scripta Materialia 56 (2007) 561-564.
19. S.M. Kwak, H.K. Park, J.M. Doh, J.K. Yoon, S.J. Lee, I.J. Shon, Journal of Ceramic Processing Research, 14 (2013) 65-69.
20. I.J. Shon, K.I. Na, W. Kim, J.W. Lim, J.M. Doh, J.K. Yoon, Journal of Ceramic Processing Research, 13 (2012) 272-277.
21. H.S. Kang, J.M. Doh, J.K. Yoon, B.J. Park, I.J. Shon, Korean J. Met. Mater. 50 (2012) 891-896.
22. C.Suryanarayana, M.Grant Norton, X-ray Diffraction A Practical Approach, Plenum Press, New York, 1998.
23. Z. Shen, M. Johnsson, Z. Zhao and M. Nygren, J. Am. Ceram. Soc. 85 (2002) 1921-1927.
24. J. E. Garay, U. Anselmi-Tamburini, Z. A. Munir, S. C. Glade and P. Asoka- Kumar, Appl. Phys. Lett. 85 (2004) 573-575.
25. J. R. Friedman, J. E. Garay. U. Anselmi-Tamburini and Z. A. Munir, Intermetallics. 12 (2004) 589-597.
26. J. E. Garay, J. E. Garay. U. Anselmi-Tamburini and Z. A. Munir, Acta Mater. 51 (2003) 4487-4495.
27. K. Niihara, R. Morena, and D. P. H. Hasselman, J.Mater. Sci. Lett. 1 (1982) 12-16.